Topographic Correlations within Lunar Swirls in Mare Ingenii

Deborah Domingue[1], John Weirich[1], Frank Chuang[1], Amanda Sickafoose[1], Eric Palmer[1],

Planetary Science Institute, 1700 E. Fort Lowell, Suite 106, Tucson, AZ 85719-2395, USA.

Corresponding author: Deborah Domingue (domingue@psi.edu)

Key Points:

- Meter-scale topographic correlations between on- and off-swirl regions discovered in Mare Ingenii
- Topographic correlations suggest dust migration is involved in lunar swirl formation

Abstract

The Moon's bright albedo markings, known as swirls, are defined by broad, bright, on-swirl areas separated by darker off-swirl lanes. Their formation mechanism has long been debated and is key for understanding the processing of the lunar surface, the mobility of the lunar soil particles, and the effects of the space environment on planetary surfaces. Here we present, for the first time, evidence that these features do not necessarily cross the surface without regard to topography or local terrain. Within portions of Mare Ingenii on the lunar far-side, brighter on-swirl areas have statistically lower mean elevations than adjacent, darker, off-swirl lanes. These topographic characteristics provide constraints on the plausible formation mechanisms for the swirls in Mare Ingenii, which in turn provide insight into lunar soil migration and evolution. We believe this correlation with topography argues for highly mobile dust transport across the lunar surface.

Plain Language Summary

Statistically significant correlations in elevation between on- and off-swirl regions within Mare Ingenii are apparent in meter-scale resolution topographical data.

1 Introduction

Lunar swirls are associated with local crustal magnetic anomalies (Hood et al. 1979, Hood and Schubert 1980), though not all magnetic anomalies display swirl albedo markings (Blewett et al. 2011, Denevi et al. 2016) and in some swirl regions, the distinctive albedo markings extend into non-magnetic regions (Syal and Schultz 2015). There is no apparent correlation of magnetic field strength with the presence of swirls (Blewett et al. 2011, Denevi et al. 2016) nor are there any correlations in the magnitude of the albedo difference between on-swirl and dark off-swirl lanes with magnetic field strength (Syal and Schultz 2015). However, preliminary correlations between OH/H_2O spectral markers and field strength have been noted (Hess et al. 2020). These magnetic fields create mini-magnetospheres (Halekas et al. 2008) capable of deflecting solar wind protons from the surface (Lue et al. 2011), thus providing an explanation for the correlation between OH/H_2O and field strength. Modeling of the magnetic field associated with the Reiner Gamma swirl indicates that the field lines are predominantly horizontal over the bright, on-swirl areas and vertical over the darker lanes (Hemingway and Garrik-Bethell 2012).

Viable swirl formation models must explain their association with magnetic anomalies and their properties, in addition to the spectral properties of bright on-swirl and dark lane areas versus the nearby, background, lunar regolith. The lunar surface has been matured over time by interactions with the solar wind and impacts from micrometeoroids, collectively referred to as space weathering. The spectral evolution of lunar soils with space weathering involves a decrease in absorption band strengths, a wavelength-dependent darkening resulting in a red spectral slope in the visible to near-infrared (Vis-NIR, e.g. Hapke 2001), and a wavelength-dependent brightening resulting in a blue spectral slope in the ultraviolet to visible (UV-Vis, e.g. Hendrix et al. 2016). While on-swirl areas display some spectral characteristics similar to fresh impact craters and ejecta (Denevi et al. 2016), indicative of less mature soil (Bell and Hawke 1981, Blewett et al. 2011, Kramer et al. 2011a, Denevi et al. 2016, 2014, Glotch et al. 2015, Hendrix et al. 2015), analysis of the spectral properties of the Mare Ingenii and Reiner Gamma swirl regions using M^3 data show that the swirl regions do not follow the spectral trends associated with typical soil maturation nor are they consistent with immature regolith (Pieters et al. 2014, 2021, Pieters and

Noble 2016). Swirl regions also do not represent a mixture of local components; they display their own distinctive spectral properties (Pieters et al. 2014, Pieters and Nobel 2016). Case in point: bright on-swirl regions display very little difference in absorption band strength compared to dark lanes and nearby mature soils (Pieters and Noble 2016), in addition to a wavelength-independent increase in albedo (Pieters et al. 2014, 2021, Pieters and Noble 2016). However, measures of optical maturity using reflectance versus reflectance ratio properties in the Vis-NIR (Lucey et al. 2000a,b) show they are less mature than the dark lanes (Kramer et al. 2011a, Lemelin et al. 2019).

On-swirl regions are higher in feldspar and orthopyroxene (Lemelin et al. 2019) and are depleted in FeO (Lemelin et al. 2019), TiO_2 (Sato et al. 2017), and OH (Kramer et al. 2011b, Hess et al. 2020). Of particular interest, is the abundance of submicroscopic ($\leq$ 1μm) iron particles. It is the presence of these particles, created through both solar wind ion and micrometeorite bombardment, which cause the spectral changes ascribed to space weathering. These particles fall into two categories, nanoscale (<~40 nm) and microscale (>~40 nm), each affecting the spectral properties differently. Radiative transfer modeling indicates that the on-swirl regions contain significantly lower abundances of nanoscale iron than surrounding soils, but similar abundances of microscale iron (Trang and Lucey 2019). This is based on the assumption of a uniform grain size and particle density across the lunar surface (Trang and Lucey 2019). Spectral analyses in the near-ultraviolet (NUV) through the near-infrared (NIR) also support the lower abundance of nanoscale iron in the on-swirl regions compared to the nearby, normal mature regolith, with the added constraint of an increased deficiency in the smaller (<~15nm) size range (Blewett et al. 2021). In contrast, examination of M^3 spectra of Reiner Gamma by Pieters et al. (2021) supports a decrease in the micron-sized size fraction as opposed to the nanoscale size fraction.

Compaction can also cause variations in brightness. More compact soils display a higher albedo without any changes to the spectral slope or absorption band depths. Hess et al. (2020) examined regolith compaction within swirl regions and found on-swirl areas were more compact.

Several processes are proposed to explain swirl formation: 1) magnetic shielding of the surface from the solar wind to retard soil maturation (Hood et al. 1979, Hood and Schubert 1980, Hood and Williams, 1989), 2) levitation and transport of fine-grained dust through electrostatic charging (Garrick-Bethall et al. 2011, Pieters and Gerrick-Bethall 2015), 3) sorting and relocation of darker, magnetized materials (Pieters and Gerrick-Bethall 2015), and 4) surface scouring by comet impacts (Schultz and Srnka 1980, Syal and Schultz 2015, Pinet et al. 2000, Starukhina and Shkuratov 2004). Each process has both supporting and contra-indicating evidence. Here we present a newly discovered topographic correlation between on- and off-swirl regions within Mare Ingenii that may illuminate the relative roles of these processes in forming swirls.

The evidence shows that variations in composition and compaction of the optically active portion (top few micro- to milli-meters) play a role in the swirl albedo patterns, in addition to surface interactions with the local magnetic field. Topography can affect the compositional and size segregation of materials and sustain them for geologically significant time scales. The observed

topographic correlation may be key in resolving and interpreting these observational properties and understanding the relative contributions of these swirl formation processes.

2 Methods and Approach

The Mare Ingenii swirls (33.7° S, 163.5° E) are located within the southwest corner of the Ingenii basin. Two study areas (A and B; Figures 1 & 2, respectively) were chosen for detailed examination. Study area A represents a more diffuse, lower-contrast albedo boundary and study area B represents a sharper, higher-contrast albedo boundary.

Digital elevation models (DEM) of the two study areas were created using Lunar Reconnaissance Orbiter Camera (LROC) narrow angle camera (NAC) images empolying stereophotoclinometry techniques (Gaskell 2008, Palmer et al. 2016) (S1). Stereophotoclinometry combines the highly accurate absolute position of a stereo solution, with the high-resolution relative position of a photoclinometric solution. Stereo heights were determined every 50-60 m and all other heights were determined by photoclinometry relative to the stereo height. DEMs of both study areas at 70-80 cm/pixel vertical and horizontal resolutions were derived from the imaging data set.

Regional slopes of up to 0.5° in both study areas were identified and corrected to prevent slope bias. Individual impact craters down to 50 m diameter and other larger topographically distinct geologic features were identified, mapped, and their areas masked from the slope-corrected data to remove extreme high and low elevation values from both on-swirl and dark lane sub-regions (Fig. 1 & 2, S2). The final elevation values within defined on- and off-swirl (dark lane) sub-regions in each study area were then exported for statistical analyses. For study area A, two concentric off-swirl sub-regions were defined, each with a comparable number of data points to the on-swirl sub-region. For study area B, the on-swirl and a single, off-swirl dark lane sub-region cover the full study area. The mapped boundaries between on- and off-swirl sub-regions should be considered approximate due to varying, and often subtle, albedo contrast in the images.

To investigate the topographic data, we compared cumulative distributions between on-swirl and off-swirl locations within each study area. This method retains more information than standard histogram binning, which has arbitrary boundaries, and it provides a straightforward graphical representation of key characteristics and distribution shapes. We evaluated the statistical significance of the topographic differences between on- and off-swirl (dark lane) sub-regions using Kuiper's variant of the Kolmogorov-Smirnov (K-S) test (Press et al. 2007). When dealing with large datasets, even small differences in distributions can become statistically significant.

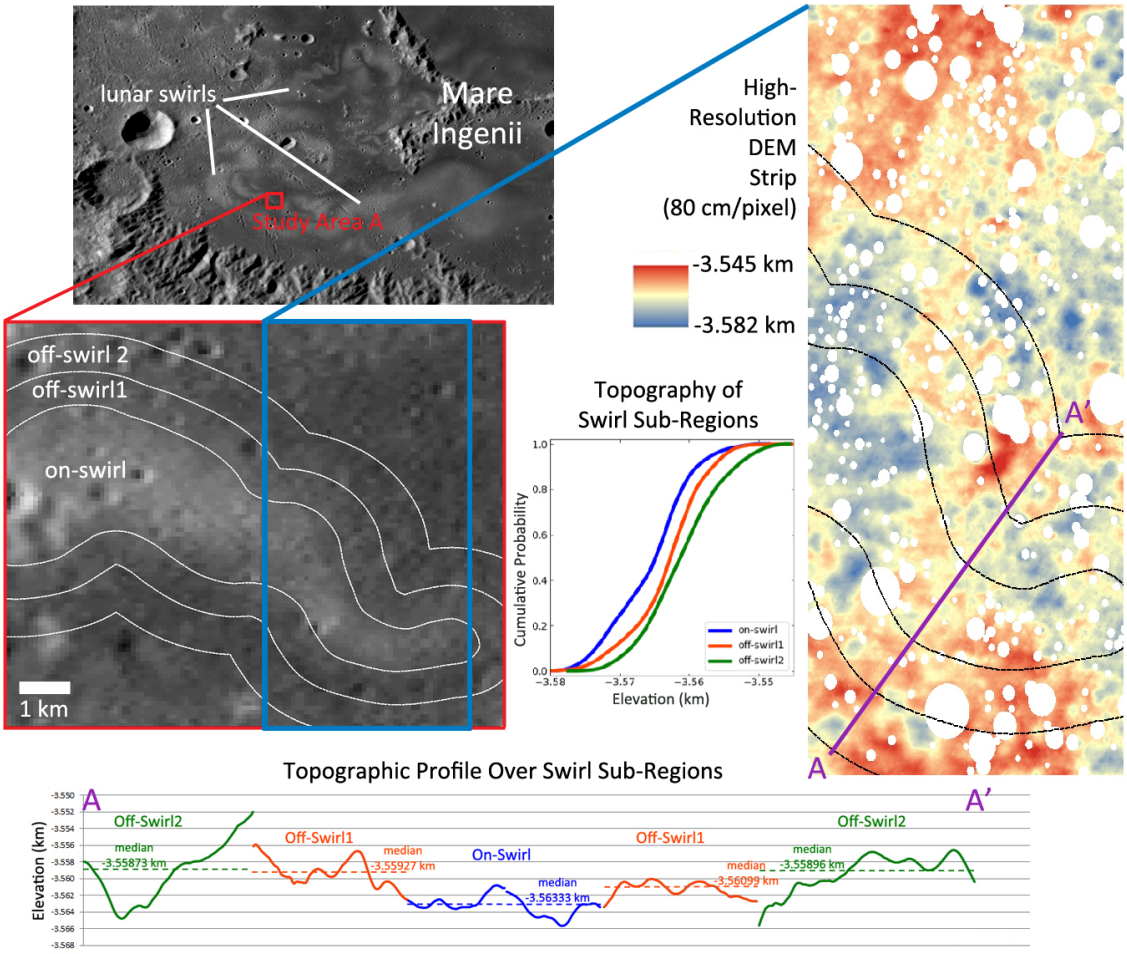

3 Results

The topographic distributions for each of the high-resolution study areas are plotted in Figs 1 & 2. The K-S test results represent a confidence level of greater than 4 sigma that the on- and off-swirl topographic datasets are not drawn from the same samples at either study area. In study area A, 98% of the on-swirl data are lower than the inner, off-swirl1 and outer, off-swirl 2 data. In study area B, 99% of the on-swirl data are lower than the off-swirl data. For study area A, the mean of the on-swirl heights is 2.386±0.005 m lower than off-swirl1 and 4.475±0.005 m lower than off-swirl2; implying a progressive degradation in elevation from off- to on-swirl. For study area B, the mean of the on-swirl heights is lower than the off-swirl, dark lanes by 2.640±0.004 m.

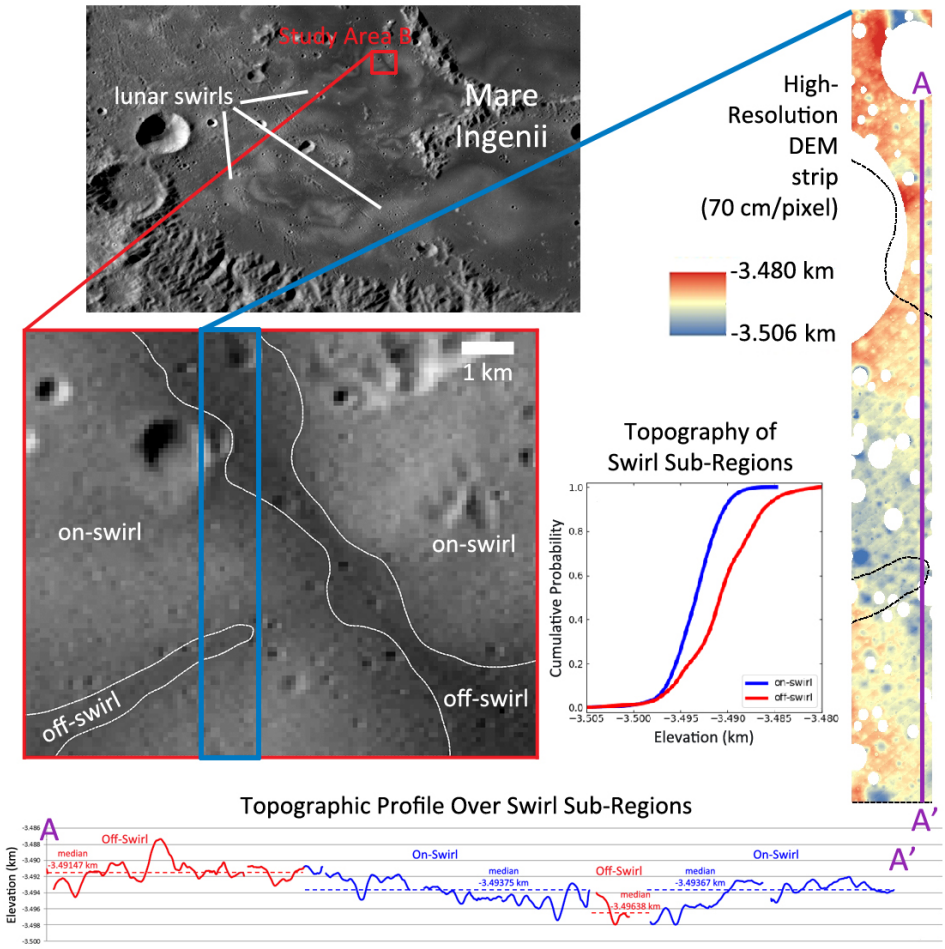

Histograms of the topographic data, with fits (Fig. 3), show the best-fit Gaussian means to the topographic data are lower in the on-swirl sub-region in study area A by 2.7±0.4 m compared to the inner, off-swirl1 sub-region and by 3.7±0.4 m compared to the outer, off-swirl2 sub-region. Similarly, the best-fit Gaussian means for study area B show the topographic data are lower in the on-swirl sub-region by 2.7±0.2 m compared to the off-swirl, dark lanes. These fits to the binned data provide a second measurement of the differences in the height distributions and are confirmation that the on-swirl sub-regions are indeed lower than their surroundings by a few meters.

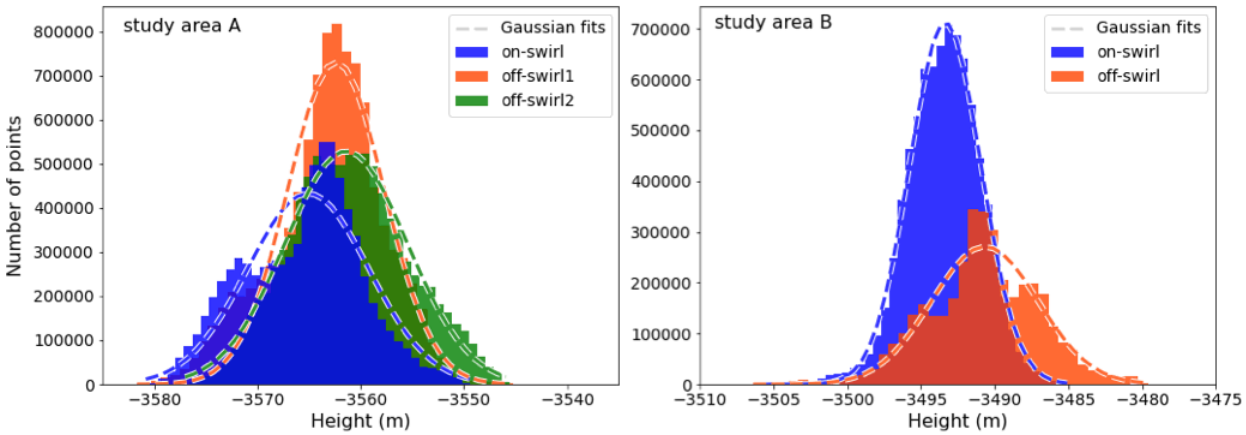

5 Discussion

Stereophotoclinometry has enabled the measurement of lunar topographic features at sub-meter scale both horizontally and vertically. In contrast, the lunar digital elevation model derived from the Lunar Orbiter Laser Altimeter (LOLA) and SELENE Terrain Camera has a resolution of 3 – 4m (Baker et al. 2016a), which would not detect the topographic differences discovered here using the stereophotoclinometric technique. These topographic lows form 'pockets' for trapping and enabling the collection of sub-micron to micron-sized dust, the size fraction that most highly affects the spectral properties (Pieters 1993). However, in order to trap lunar dust grains, there must first be a mechanism for migrating lunar dust across the Moon's surface.

Lunar dust can be electrostatically levitated and transported on the Moon, as charged particles interact with the near-surface plasma environment (Colwell et al. 2007). Many studies infer that dust is lofted predominantly in the terminator region (Garick-Bethell et al. 2011) but observations (Severnyi et al. 1975, Page and Carruthers 1978) and theory (Singer and Walker 1962a,b, Walker 1973, Stubbs and Farrell 2006) suggest lofting may occur globally, enabling global dust migration. The sizes of lofted particles are not well constrained. Cohesive forces are likely to dominate dust grains 1–1000 μm in size and prevent them from detaching from the surface (Hartzell and Scheeres 2011); however, the repulsive force generated in the patched-charge model is sufficient to loft particles tens of microns in diameter (Wang et al. 2016, Schwan et al. 2017). In addition, the presence of a magnetic field can cause magnetic mirroring, a phenomenon where solar wind electrons are preferentially reflected while solar wind protons penetrate deeper within the magnetic field. The different penetration depths between the solar wind electrons and protons create a charge separation near the surface. This unique environment can attract or repel charged dust into or out of the swirls (Pieters and Garrick-Bethell 2015). Thus while there are multiple methods for transporting dust; one is directly correlated to the magnetic field presence at lunar swirls.

Numerical simulations of electrostatic dust transport in a photoelectron sheath near a 7-m diameter, 1-m deep crater, show that dust grains accumulate within the crater due to more complex electric fields associated with the crater's edge (Poppe et al. 2012). The crater in this simulation can be thought of as a 'topographic pocket', analogous to the topographic lows associated with the on-swirl regions, albeit slightly shallower. Poppe et al.'s (2012) study shows

that dust can migrate into the crater and be trapped. In transport simulations with dust grains ranging from 10 nm to 10 μm, the crater pocket traps larger grains at higher efficiency than smaller grains due to the varying relative balance between electrostatic and gravitational forces as a function of grain size (Poppe et al. 2012).

The topographic pocket need not be a crater, any depression can serve to trap and accumulate dust. In the case of the swirl regions, there are a few caveats to this extrapolation for dust entrapment. Swirl regions represent a different plasma environment than that considered in the simulations, and the presence of a magnetic field on electrostatically levitated dust has not been examined. The change in slope of the topography from the crater's rim is steeper than the topographic slope change between on- and off-swirl. The boundary in swirl regions can be very gradational or diffuse compared to a crater's rim. This is seen in Swirl Area B (Fig. 2), where the tip of the off-swirl 'tongue' near A' is close in albedo to the adjacent on-swirl region, and may represent a transitional area between on- and off-swirl. Simulations taking these differences into account are beyond the scope of this study, however photometric studies support the structural differences expected from the entrapment of fine-grained dust.

Photometric studies of lunar swirl regions suggest millimeter-scale roughness and compaction differences between on- and off-swirls (Pinet et al. 2000, Kreslavsky and Shkuratov 2003, Kaydash et al. 2009, Baker et al. 2016b, Hess et al. 2020), ascribed to the removal of fine-grained lunar dust and the destruction of the fairy-castle structure of the lunar soils (Syal and Schultz 2015, Wu and Hapke 2018). This has been used to argue for comet impact as the formation mechanism of lunar swirls. Alternatively, if magnetic mirroring lofts and removes the fine-grained fraction from those bright areas where the magnetic field is parallel to the surface, then this could disrupt the fairy-castle structure and also be commensurate with the difference in compaction derived by Hess et al. (2020). Electrostatic dust transport simulations also constrain the relative grain size of the lunar dust trapped in the on-swirl pockets compared to the off-swirl regions, in addition to affecting the soil roughness and compaction due to the deposition process. These constraints, combined with Poppe et al.'s (2012) transport simulation results, imply that it is not the very finest fraction (< 1 μm) of the lunar dust that is trapped in the on-swirl topographic pockets, but a larger size-fraction (> 10 μm) dust grain that would form a soil structure less porous than the fairy-castle structure ubiquitous to the lunar surface. The finest fraction could continue to migrate globally across the lunar surface until it encounters a trap 10s to 100s of meters deep (Colwell et al. 2007), such as some of the craters within the swirl regions. Roughness measurements derived from LRO's Mini-RF synthetic aperture radar (SAR) observations detect no surface roughness variations within swirl regions at the centimeter- to decimeter-scale (Neish et al. 2011), thus the soil structure differences are at the micrometer to millimeter scale sensitivity of the spectral and photometric measurements. These observations argue that the swirl albedo pattern is shallow and consistent with a very thin surface layer less than several decimeters thick (Neish et al. 2011), providing a constraint on the depth of the dust layer that can accumulate within the on-swirl topographic pockets.

Swirl formation mechanisms must also explain the maturity and compositional properties. Maturity measurements support surface shielding from the solar wind, as does the orientation of the fields with respect to bright and dark areas, the abundance of OH/H_2O of bright areas relative to the nearby, background surface (Kramer et al. 2011a, Hess et al. 2020), and the correlation of

OH/H_2O abundance with magnetic field strength (Hess et al. 2020). These same observed properties also support the removal of the uppermost, very thin, mature layer of the regolith by cometary gas, leaving behind a less mature regolith that will undergo reduced space weathering due to magnetic shielding (e.g. Hess et al. 2020). While there is evidence supporting a role for magnetic shielding in swirl formation, the spectral signatures require the inclusion of additional physical processes (Pieters et al. 2014, 2021, Pieters et al. 2016, Hess et al. 2020). For example, the on-swirl areas display steeper NIR continuum slopes and shallower NUV slopes than fresh material from background lunar regolith (Blewett et al. 2021). The newly detected topographic correlations in this study argue for contributions from grain sorting; by electrostatic levitation, magnetic sorting, or both.

The associated magnetic fields reduce the interaction of the solar wind with the surface on the order of 10 – 50% (Saito et al. 2010; Wieser et a. 2010; Lue et al. 2011). The time scales for the two dominate space-weathering processes are 10^4 – 10^6 years for solar wind radiation and, 10^8 – 10^9 years for micrometeorite bombardment (Vernazza et al. 2009). Each of these weathering processes produces rims on the soil grains. Examination of solar flare track density measurements for mature lunar soils indicate both types of rims accumulate in ~ 10^6 – 10^7 years (Keller and Zhang 20156; Pieters and Nobel 2016), suggesting that neither process dominates the maturation process. These time scales are much smaller than the 2 – 4 billion year age of the background surface of most swirls (e.g. Garrick-Bethall et al. 2011), and the accumulation of the weathering rims is also shorter than the < 10^8 yr age of the cross-cutting relationships observed in some swirl regions (Schultz and Srnka 1980, Syal and Schultz 2015). Even with a reduction of solar wind radiation by 50%, the surface in swirl regions will have been exposed to the weathering environment over a sufficient time span to have optically matured unless there is a mechanism for refreshing the surface. The timescales for dust migration over distances corresponding to swirl region scales are not constrained by current observations or models, nor are the lifetimes for dust grains within the on-swirl topographic pockets or dust traps. It is feasible that migration of dust into these traps operates on timescales shorter than the solar wind maturation process (Garrick-Bethell et al. 2011), thus the accumulated lunar dust has been sufficiently shielded from the solar wind to explain the swirl maturity properties.

Compositionally, on-swirl regions are enriched in feldspar and orthopyroxene (Lemelin et al. 2019), depleted in nanoscale iron (Trang and Lucey 2019; Blewett et al. 2021), and show an abundance of microscale iron comparable to the background regolith (Trang and Lucey 2019; Blewett et al. 2021). Feldspathic and agglutinitic (impact-glass welded conglomerates of soil grains) material within lunar soils increases with decreasing particle size for all lunar soil types (Pieters 1993, Pieters and Taylor 2003). The brighter, feldspar enriched lunar dust (<25 μm) (Pieters 1993) is the easiest to electrostatically transport (Garrick-Bethell et al. 2011, Pieters and Garrick-Bethell 2015). Their interaction with the swirl's magnetic field provides a potential mechanism for on-swirl feldspar enrichment (Garrick-Bethell et al. 2011, Pieters and Garrick-Bethell 2015) in the larger (>10 μm) size range. However, this fine-fraction (< 25 μm diameter) has also been demonstrated to be highly mature (Pieters et al. 1993). Therefore, the accumulation of lunar dust 1- 25 μm in diameter within the on-swirl pockets seemingly contradicts the relative maturity measures observed for swirl regions, though those maturity correlations have been disputed (Pieters et al. 2014, 2021; Pieters and Noble 2016). This contradiction can be resolved if there is a mechanism to remove the more weathered fraction.

The weathered fraction of the lunar soil contains submicroscopic iron. Studies of anorthite (Ca-rich endmember feldspar) suggest that micrometeorite bombardment dominates the production of nanoscale iron (Keller and Zhang 2015; Trang and Lucey 2019), and thus at first glance would suggest this size fraction of submicroscopic iron should be the same on-swirl as in the background regolith, commensurate with the studies of Pieters et al. (2021), but contradictory to the works of Trang and Lucey (2019) and Blewett et al. (2021). However, the presence of nanoscale iron would magnetize these grains, and be of sufficiently low density to be most susceptible to removal by magnetic sorting, or a combination of electrostatic levitation and magnetic removal. The larger, heavier, microscale grains (such as those found in agglutinates) may not be removed, thus explaining their similar concentration on-swirl as off-swirl. Thus, the on-swirl pockets may be more effective at accumulating the less mature component of the lunar soil's dust while the dark off-swirl regions form a repository for the more mature fraction.

Questions that remain, and would benefit from laboratory and theoretical work beyond the scope of this study, include:

- What is the size/density fraction of grains preferentially trapped in on-swirl pockets?
- How does this size/density fraction compare to those grains that would be preferentially trapped in craters within the swirl regions?
- If the lofted grains are magnetic, how does the magnetic field affect where they are deposited?
- How does the deposition of these lofted materials affect the compaction/porosity of the regolith?

6 Conclusions

The topographically low, higher-albedo, on-swirl regions observed in Mare Ingenii support that the migration of dust across the lunar surface contributes to swirl formation, which is consistent with the spectral and photometric properties. For two study areas in the Mare Ingenii swirls, we find that the bulk topography is 2-3 m lower on swirl than in the immediate surrounding dark lanes. The on-swirl regions serve as traps for intermediate-sized (10 - 1000 μm) lunar dust grains. Within these traps, the grain size and deposition process form a more compact soil structure compared to the average lunar surface.

Acknowledgments

This work was supported by NASA's Lunar Data Analysis Program (80NSSC17K0278) and the Solar System Exploration Research Virtual Institute 2016 (SSERVI16) Cooperative Agreement (NNH16ZDA001N) SSERVI-TREX.

Data Availability Statement

Data used include Lunar Reconnaissance Orbiter Narrow Angle Camera (LROC-NAC) images. The specific images used are listed in the supplementary materials. These images are publically available through the Planetary Data System Cartography and Imaging Sciences Node (pds-imaging.jpl.nasa.gov).

The compositional and optical maturity maps are available from the LROC Quickmap public site (https://quickmap.lroc.asu.edu/).

The stereophotoclinometry technique and software is described in Gaskell 2008 and Palmer et al. 2016.

Gaskell, R.W., 2008. Characterizing and navigating small bodies with imaging data. Meteoritics & Planetary Sci. 43, Issue 6, 1049 – 1061.

Palmer, E.E., Head, J.N., Gaskell, R.W., Sykes, M.V., McComas, B., 2016. Mercator Independent rover localization using stereophotoclinometry and panoramic images. Earth and Space Sci. 3, Issue 12, 488 – 509.

The data products examined in this study are part of a larger project and will be archived with the Planetary Data System at the completion of the project.

References

Adams, J.B., McCord, T.B.,1973. Vitrification in the lunar highlands and identification of Descartes material at the Apollo 16 site. In: Proceedings of the 4th Lunar Science Conference, pp. 163–177.

Barker, M.K., 2016. A nuew lunar digital elevation model from the Lunar Orbiter Laser Altimeter and SELENE Terrain Camera. Icarus 273, 346 – 355.

Bell, J.F., Hawke, B.R., 1981. The Reiner Gamma formation: Composition and ori- gin as derived from remote sensing observations. In: Proceedings of 12th Lunar Planetary Science, pp. 679–694.

Blewett, D.T., et al., 2011. Lunar swirls: Examining crustal magnetic anomalies and space weathering trends. J. Geophys. Res. 116 (E02002). doi: 10.1029/2010JE004656.

Blewett, D.T., Denevi, B.W., Cahill, J.T.S., Klima, R.L., 2021. Near-UV and near-IR reflectance studies of lunar swirls: Implications for nanosize iron content and the nature of anomalous space weathering. Icarus 364, doi:10.106/j.icaurs.2021.114472.

Clegg, R.N., Jolliff, B.L., Robinson, M.S., Hapke B.W., Plescia, J.B., 2014. Effects of rocket exhaust on lunar soil reflectance properties. Icarus 227. 176 – 194.

Colwell, J. E., Batiste, S., Horanyi, M., Robertson, S., Sture, S., 2007. Lunar Suface: Dust Dynamics and Regolith Mechanics. Reviews of Geophysics. 45, 2005RG000184.

Denevi, B.W., et al., 2014. Characterization of space weathering from Lunar Reconnaissance Orbiter Camera ultraviolet observations of the Moon. J. Geophys. Res. Planets 119 (5). doi: 10.10 02/2013JE0 04527.

Denevi, B.W., et al. 2016. The distribution and extent of swirls. Icarus 273, 53 – 67.

Garrick-Bethell, I., Head, J.W., Pieters, C.M., 2011. Spectral properties, magnetic fields, and dust transport at lunar swirls. Icarus 212 (2), 4 80–4 92. doi: 10.1016/j.icarus. 2010.11.036.

Gaskell, R.W., 2008. Characterizing and navigating small bodies with imaging data. *Meteoritics & Planetary Sci.* 43, Issue 6, 1049 – 1061.

Glotch, T.D., et al., 2015. Formation of lunar swirls by magnetic field standoffof the solar wind. Nat. Commun. 6, 6189. doi: 10.1038/ ncomms7189.

Halekas, J.S., et al., 2008. Density cavity observed over a strong lunar crustal magnetic anomaly in the solar wind: a mini- magnetosphere? Planet. Sp. Sci. 56 (7), 941–946. doi: 10.1016/j.pss.2008.01.008.

Hartzell, C. M. and D. J. Scheeres, 2011. The role of cohesive forces in particle launching on the Moon and asteroids, Plan. Space Sci., 59.

Hemingway, D., Garrick-Bethell, I., 2012. Magnetic field direction and lunar swirl morphology: Insights from Airy and Reiner Gamma. J. Geophys. Res. 117 (E10), E10012. doi: 10.1029/2012JE004165.

Hendrix, A.R., et al. 2012. The lunar far-UV albedo: Indicator of hydration and weathering. J. Geophys. Res. 117, E12001, doi:10.1029/2012JE004252.

Hendrix, A.R., et al. ,2015. Far-ultraviolet characteristics of lunar swirls. In: Proceedings of Lunar Planetary Science Conference 46.

Hess, M., et al. 2020. Processes governing the VIS/NIR spectral reflectance behavior of lunar swirls. A&A 639, A12. doi:10.1051/0004-6361/201937299.

Hood, L.L., Coleman, P.J., Wilhelms, D.E., 1979. Lunar nearside magnetic anomalies. In: Proceedings of 10th Lunar Planetary Science Conference, pp. 2235–2257.

Hood, L.L., Schubert, G., 1980. Lunar magnetic anomalies and surface optical properties. Science 208, 49–51.

Hood, L.L., Williams, C.R., 1989. The lunar swirls: Distribution and possible origins. In: Proceedings of 19th Lunar Planetary Science Conference, pp. 99–113.

Kaydash, V., et al., 2009. Photometric anomalies of the lunar surface studied with SMART-1 AMIE data. Icarus 202 (2), 393–413. doi: 10. 1016/j.icarus.2009.03.018.

Kramer, G.Y., et al., 2011a. Characterization of lunar swirls at Mare Ingenii: A model for space weathering at magnetic anomalies. J. Geo- phys. Res. 116 (E4), E04008. doi: 10.1029/2010JE003669.

Keller, L.P., McKay, D.S., 1993. Discovery of vapor deposits in the lunar regolith. Science 261, 1305–1307.

Keller, L.P., McKay, D.S., 1997. The nature and origin of rims on lunar soil grains. Geochim. Cosmochim. Acta 61, 2331–2341.

Keller, L. P., and S. Zhang (2015), Rates of space weathering in lunar soils, Abstract 2056 presented at Workshop on Space Weathering of Airless Bodies: Integration of Remote Sensing Data, Laboratory Experiments, and Sample Analysis, Lunar and Planet. Inst., Houston.

Keller, L.P., et al. 2000. Space weathering in the fine size fraction of lunar soils: Mare/highland differences (abstract). Lunar Plnaet. Sci. 31, #1655. Lunar and Planetary Institute, Houston, Texas, USA.

Kramer, G.Y., et al., 2011b. M3 spectral analysis of lunar swirls and the link between optical maturation and surface hydroxyl formation at magnetic anomalies. J. Geophys. Res. 116, E00G18, doi:10.1029/2010JE003729.

Kreslavsky, M.A., Shkuratov, Y.G., 2003. Photometric anomalies of the lunar sur- face: Results from Clementine data. J. Geophys. Res. 108 (E3), 5015. doi: 10.1029/ 20 02JE0 01937.

Lemelin, M., et al., (2019) The compositions of the lunar crust and upper mantle: Spectral analysis of the inner rings of lunar impact basins, Planetary and Space Science, vol. 165, p. 230-243.

Lue, C., et al., 2011. Strong influence of lunar crustal fields on the solar wind flow. Geophys. Res. Lett. 38 (3), L03202. doi: 10.1029/ 2010GL046215.

Lucey, P.G., et al., 2000a. Imaging of lunar surface maturity. J. Geophys. Res. 105 (E8), 20377–20386.

Lucey, P.G., et al., 2000b. Lunar iron and titanium abundance al- gorithms based on final processing of Clementine ultraviolet-visible images. J. Geophys. Res. 105 (E8), 20297–20305. doi: 10.1029/1999JE001117.

Neish, C.D., et al., 2011. The surficial nature of lunar swirls as revealed by the Mini-RF instrument. Icarus 215 (1), 186–196. doi: 10. 1016/j.icarus.2011.06.037.

Page, T.T., Carruthers, G.R., 1978. Far ultraviolet atlas of the large Magellanic Cloud. Naval Research Laboratory Report 8206, 1–131.

Palmer, E.E., Head, J.N., Gaskell, R.W., Sykes, M.V., McComas, B., 2016. Mercator-Independent rover localization using stereophotoclinometry and panoramic images. Earth and Space Sci. 3, Issue 12, 488 – 509.

Pieters, C.M., 1993. Optical effects of space weathering: The role of the finest fraction. J. Geophys. Res. 98 (E11), 20817–20824.

Pieters, C.M., 2000. Space weathering on airless bodies: Resolving a mystery with lunar samples. Meteor. Planet. Sci. 35, 1101–1107.

Pieters, C.M., Garrick-Bethell, I., 2015. Hydration variations at lunar swirls. Lunar Planetary Science 46, Abstract 2120.

Pieters, C.M., and Noble, S.K., 2016. Space weathering on airless bodies. J. Geophys. Res. Planets, 121, doi:10.1002/2016JE005128.

Pieters, C.M., Donaldson Hanna, K.L., Sunshine, J.M., Garrick-Bethell, I., New M-Cube insights on the character of the mysterious Reiner Gamma swirls. Lunar and Planetary Science Conf. 2021. NO. 2548.

Pieters, C.M., Moriarty III, D.P., Garrick-Bethell, I., 2014. Atypical regolith processes hold the key to enigmatic lunar swirls. Lunar Planetay Science 45, Abstract 1408.Pieters, C., Taylor, L., 2003. Systematic global mixing and melting in lunar soil evolution. Geophys. Res. Lett. 30, 2048.

Pinet, P.C., et al., 2000. Local and regional lunar regolith characteristics at Reiner Gamma Formation: Optical and spectroscopic properties from Clementine and Earth-based data. J. Geophys. Res. 105 (E4), 9457–9475. doi: 10.1029/1999JE001086.

Poppe, A. R., Piquette, M., Likhanskii, A., Horányi, M., 2012. The effect of surface topography on the lunar photoelectron sheath and electrostatic dust transport. Icarus. 221, 135-146.

Press, W.H., Teukolsky, S.A., Vetterling, W.T., Flannery, B.P., 2007. Numerical Recipes: The Art of Scientific Computing, third ed. University Press, Cambridge.

Sato, H., 2017. Lunar mare TiO2 abundances estimated from UV/Vis reflectance. Icarus 296, 216 – 238.

Schwan, J., et al., 2017. The charge state of electrostatically transported dust on regolith surfaces, GRL, 44.

Severnyi, A.B., Terez, E.I., Zvereva, A.M., 1975. The measurements of sky brightness on Lunokhod-2. Moon 14, 123–128.

Singer, S.F., Walker, E.H., 1962a. Electrostatic dust transport on the lunar surface. Icarus 1, 112–120.

Singer, S.F., Walker, E.H., 1962b. Photoelectric screening of bodies in interplanetary space. Icarus 1, 7–12.

Starukhina, L.V. and Shukratov, Y.G., 2004. Swirls on the Moon and Mercury: meteoritd swarm encounters as a formation mechanism. Icarus 167, 136 – 147. doi:10.1016/j.icarus. 2003.08.002.

Stubbs, T. J., Farrell, W. M., 2006. A Dynamic Fountain Model for Lunar Dust. Advances in Space Research. 37, 59-66.

Schultz, P.H., and Srnka, L.J., 1980. Cometary collisions on the Moon and Mercury. Nature 284, 22 – 26.

Syal, M.B., Schultz, P.H., 2015. Cometary impact effects at the Moon: Implications for lunar swirl formation. Icarus 257, 194 – 206.

Trang, D., Lucey, P.G., 2019. Improved space weathering maps of the lunar surface through radiative transfer modeling of Kaguya multiband imager data. Icarus 321, 307 – 323. doi:10.1016/j.icarus.2018.11.014

Walker, E.H., 1973. The lunar electronosphere and implications for erosion on the Moon. In: Photon and Particle Interactions with Surfaces in Space, Proceedings of the 6th ESLAB Symposium, Noordwijk, pp. 521–544.

Wang, X., et al., 2016. Dust charging and transport on airless planetary bodies, Geophys. Res. Lett., 43.

Wentworth, S.J., Keller, L.P., McKay, D.S., Morris, R.V., 1999. Space weathering on the Moon: Patina on Apollo 17 samples 75075 and 76015. Meteorit. Planet. Sci. 34, 593 – 603.

Wu, Y., and Hapke, B., 2018. Spectroscopic observations of the Moon at the lunar surface. Earth Planet. Sci. Lett, 484, 145 – 153. doi:10.1016/j.epsl.2017.12.003

Figure 1. **(Upper Left)** Location of study area A (red box) with lunar swirls in Mare Ingenii. **(Middle Left)** Portion of LROC WAC mosaic with defined on-swirl and two concentric off-swirl sub-regions (off-swirl1 and off-swirl2) and the location of a high-resolution (80 cm/pixel) DEM strip (blue box). **(Middle Right)** Cumulative frequency distribution plot of the high-resolution slope-corrected and crater/feature-masked topography for on-swirl (blue), off-swirl1 (red), and off-swirl2 (green) regions. **(Upper Right)** Slope-corrected, crater-masked DEM with the location of a topographic profile perpendicular to swirl regions shown in purple. Colorized topography has an applied linear stretch over 3 standard deviations of the mean. **(Bottom)** Example topographic profile for the purple line, highlighting on- and off-swirl sub-regions, with the median elevation of each region demarcated by a dashed line. A boxcar filter 100 pixels wide was applied over the entire profile to smooth the overall shape. The vertical exaggeration is 44x.

Figure 2. (Upper Left) Location of study area B (red box) with lunar swirls in Mare Ingenii. **(Middle Left)** Portion of LROC WAC mosaic with defined on-swirl and off-swirl regions and the location of a high-resolution (70 cm/pixel) DEM strip (blue box). **(Middle Right)** Cumulative frequency distribution plot of the high-resolution slope-corrected and crater/feature-masked topography for on- (blue) and off-swirl (red) regions. **(Upper Right)** Slope-corrected, crater-masked DEM with the location of a topographic profile across all regions shown in purple. Colorized topography has an applied linear stretch over 3 standard deviations of the mean. **(Bottom)** Example topographic profile for the purple line, highlighting on- and off-swirl regions, with the median elevation of each region demarcated by a dashed line. A boxcar filter 100 pixels wide was applied over the entire profile to smooth the overall shape. Topography and albedo suggest that the smaller, central, off-swirl region area sampled in the profile may be a transition zone. The vertical exaggeration is 58x.

Figure 3. Histograms of the high-resolution topographic data, divided into forty height bins, for study areas A (**left**) and B (**right**). Gaussian fits to each of the on- and off-swirl regions are

plotted as dashed lines. The decreasing mean heights from off- to on-swirl are apparent, as are the different dataset sizes (see Supplement Table S2 for Gaussian fit parameters). The same color scheme has been used as that in the cumulative frequency distribution plots in Figs. 1 & 2: slight color variations indicate where data are overplotted.